# REPORT DOCUMENTATION PAGE

*Form Approved*
*OMB No. 0704-0188*



| **1. REPORT DATE** *(DD-MM-YYYY)* | **2. REPORT TYPE** | **3. DATES COVERED** *(From - To)* |
|---|---|---|
| 27 July 2016 | Conference Paper | 07 June 2016 – 27 July 2016 |

**4. TITLE AND SUBTITLE**
Cryogenic Impinging Jets Subjected to High Frequency Transverse Acoustic Forcing in a High Pressure Environment

**5a. CONTRACT NUMBER**

**5b. GRANT NUMBER**

**5c. PROGRAM ELEMENT NUMBER**

**6. AUTHOR(S)**
Mario Roa, S. Alex Schumaker, Doug Talley

**5d. PROJECT NUMBER**

**5e. TASK NUMBER**

**5f. WORK UNIT NUMBER**
Q0YA

**7. PERFORMING ORGANIZATION NAME(S) AND ADDRESS(ES) AND ADDRESS(ES)**

Air Force Research Laboratory (AFMC)
AFRL/RQRC
10 E. Saturn Blvd.
Edwards AFB, CA 93524-7680

**8. PERFORMING ORGANIZATION REPORT NO.**

**9. SPONSORING / MONITORING AGENCY NAME(S) AND ADDRESS(ES)**

Air Force Research Laboratory (AFMC)
AFRL/RQR
5 Pollux Drive
Edwards AFB, CA 93524-7048

**10. SPONSOR/MONITOR'S ACRONYM(S)**

**11. SPONSOR/MONITOR'S REPORT NUMBER(S)**
**AFRL-RQ-ED-TP-2016-144**

**12. DISTRIBUTION / AVAILABILITY STATEMENT**
Approved for Public Release; Distribution Unlimited. The U.S. Government is joint author of the work and has the right to use, modify, reproduce, release, perform, display, or disclose the work. PA Clearance Number: 16308 Clearance Date: 6/17/2016

**13. SUPPLEMENTARY NOTES**
For presentation at AIAA Propulsion and Energy; Salt Lake City, Utah; July 27, 2016
Prepared in collaboration with Sierra Lobo, Inc.

**14. ABSTRACT**

An experimental study has been conducted to explore the coupling between the impact waves created by impinging jets and high frequency acoustic pressure perturbations. High speed, backlit imaging was used to capture the physical response of impact waves present on impingement sheet formed by two like on like impinging jets. Dynamic mode decomposition was used to extract the natural frequencies of impact waves and isolate the spatial structures response present on the impingement sheet due to the transverse acoustic forcing. Chamber pressure and jet velocity were varied until impact waves became visually prominent. After impact waves became visually prominent, the impingement sheet was subjected to incremental pressure amplitudes in a pressure anti-node (PAN) and pressure node (PN) configurations. The results indicate that impact waves appear to vanish once a certain pressure amplitude is reached. When subjected to PAN forcing the impingement sheet size grows and decays and in-plane flapping is generated under a PN forcing.

**15. SUBJECT TERMS**
Nomenclature: DMD = Dynamic Mode Decomposition PAN = Pressure Anti-Node PN = Pressure Node

| **16. SECURITY CLASSIFICATION OF:** | | | **17. LIMITATION OF ABSTRACT** | **18. NUMBER OF PAGES** | **19a. NAME OF RESPONSIBLE PERSON** |
|---|---|---|---|---|---|
| | | | | | D. Talley |
| **a. REPORT** | **b. ABSTRACT** | **c. THIS PAGE** | SAR | 11 | **19b. TELEPHONE NO** *(include area code)* |
| **Unclassified** | **Unclassified** | **Unclassified** | | | N/A |

**Standard Form 298 (Rev. 8-98)**
**Prescribed by ANSI Std. 239.18**

# Cryogenic Impinging Jets Subjected to High Frequency Transverse Acoustic Forcing in a High Pressure Environment

Mario Roa[1]
*Sierra Lobo, Inc. Air Force Research Laboratory, Building 8451, Edwards AFB, CA, 93524*

S. Alexander Schumaker[2] and Douglas G. Talley[3]
*Air Force Research Laboratory, Building 8451, Edwards AFB, CA, 93524*

**An experimental study has been conducted to explore the coupling between the impact waves created by impinging jets and high frequency acoustic pressure perturbations. High speed, backlit imaging was used to capture the physical response of impact waves present on impingement sheet formed by two like on like impinging jets. Dynamic mode decomposition was used to extract the natural frequencies of impact waves and isolate the spatial structures response present on the impingement sheet due to the transverse acoustic forcing. Chamber pressure and jet velocity were varied until impact waves became visually prominent. After impact waves became visually prominent, the impingement sheet was subjected to incremental pressure amplitudes in a pressure anti-node (PAN) and pressure node (PN) configurations. The results indicate that impact waves appear to vanish once a certain pressure amplitude is reached. When subjected to PAN forcing the impingement sheet size grows and decays and in-plane flapping is generated under a PN forcing.**

## Nomenclature

*DMD* = Dynamic Mode Decomposition
*PAN* = Pressure Anti-Node
*PN* = Pressure Node

## I. Introduction

Impinging jet injectors are one of the many injectors type used for liquid propellant atomization in rocket engines[1-2]. Liquid rocket engines like the F-1 have successfully used like-on-like impinging jet injectors and are a preferred injector type for hypergolic and gelled-propellants[3-4]. Figure 1 shows a schematic of the flow field formed by a like-on-like impinging jets injector. In Figure 1 two cylindrical liquid jets strike each other at an angle 2Θ and from an impingement sheet. Impact waves or surface waves travel along the surface of the impingement sheet, detach, and form ligaments and droplets. These injectors are favored due to inherently simple design, potential high flow rate operation, and low manufacturing costs[1-2]. Although great operation success has been achieved with like on like impinging injectors, they do suffer from some major drawbacks. One such drawback is the high machining tolerance needed for like-on-like impingement of the two cylindrical jets. Another drawback, perhaps the most critical, is that rocket engine using impinging jets sacrifice performance in order to achieve an acceptable level of high frequency combustion instability[1].

Extensive experimental and theoretical studies have been performed on understanding the spray characteristics of these injectors, with particular attention given to the shape of the impingement sheet, the breakup length of liquid impingement sheet, and mean droplet size and distribution[4-8]. It has been well

**Figure 1. Schematic of typical like-on-like impinging jet injector. Figure is reproduced from Anderson[9].**

[1]Research Scientist, Sierra Lobo, Inc. 10 E. Saturn Blvd, Building 8451, Edwards, CA 93524, Member
[2]Research Engineer, AFRL/RQRC., 10 E. Saturn Blvd, Building 8451, Edwards, CA 93524, Senior Member
[3]Lead, Combustion Dynamic Group, AFRL/RQRC., 10 E. Saturn Blvd, Building 8451, Edwards, CA 93524, Associate Fellow

documented that the impingement sheet shows several physical characteristics depending on the operating Reynolds and Weber number[5, 9]. These physical characteristics or modes of the impingement sheet are: closed-rim, open-rim, and fully developed. Transition to either of these modes is dependent on jet velocity. Present on these modes are unstable hydrodynamic waves usually referred to as impact waves. It is theorized that these impact waves are the dominant mechanism in the impingement sheet breakup and atomization.

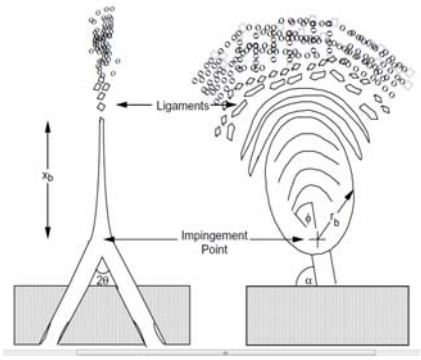


Heidmann *et al*[4] and Dombrowski *et al*[5] performed extensive studies on impinging jets under atmospheric conditions. From these studies, two mechanisms were identified as the responsible mechanism to impingement sheet breakup. One mechanism is the superposition of aerodynamic waves. The second is when waves are produced at the point of impingement, which results in ripples[8] emanating from this point. These ripples are referred to as impact waves. Impact waves were observed even in near vacuum conditions and exhibit nonlinear behavior that cannot be fully predicted by linear stability theory. Heidmann *et al* arrived at these two breakup mechanisms by systemically studying the effect of orifice diameter, jet velocity, impingement angle, pre-impingement length, and jet viscosity by using different liquid combinations of glycerol and water. Heidmann *et al* concluded that jet velocity was the parameter of choice to describe the spray structures produced by the impinging jets. Guided by Heidmann *et al* results, Dombrowski *et al* studied the disintegrations of the impingement sheet. Their results show that the disintegration of the impingement sheet usually resulted from the formation of unstable waves, either aerodynamic or hydrodynamic in origin. Their results indicate there is a transition to when impact waves control breakup of the impingement sheet. This transition occurs when the liquid jets are above a critical Weber number. This critical Weber number when impact waves start to appear lies between 65 and 165[5, 9], defined as $We = \frac{\rho v^2 D}{\sigma}$, where ρ is the jet density, v is the jet velocity, D the jet diameter, and σ is the surface tension. It should be noted that Dombrowski *et al* results are dependent on the jets being either laminar or turbulent.

Anderson *et al*[10] performed experiments on impinging jets using water at atmospheric conditions to characterize the effect of impact waves on the atomization process. Anderson *et al* measured atomization frequency from the impingement sheet using high-speed videos. They did this by monitoring a fixed point in the high speed videos and checking if ligaments and droplets passed through. They discovered that impact waves are formed with a characteristic wavelength of about one jet diameter. The experimental results also suggested that impact waves seem to dominate the atomization process over most of the conditions relevant to rocket engines and are responsible for the atomization frequency. Although, these observations was made only when jet velocities were low. Anderson *et al* also reported that the experimental results are dependent if the jets are laminar or turbulent, similar to Dombrowski *et al*.

Chen *et al*[10] performed a numerical study on the physical mechanism of impact waves and mixing process, and atomization of impinging jets. Chen *et al* carried out his numerical studies by varying Reynolds number, surface tension, and impingement sheet thickness. Chen *et al* concluded that impact waves form when the impinging jets have a Strouhal value of 0.86. Their results show that impact waves are caused by the interfacial shear stress which form capillary waves on the either side of the impingement sheet.

A single like-on-like impinging jet injector, machined at relevant dimensions for liquid rockets engines, was studied under acoustic perturbations. Cryogenic nitrogen was used as the working fluid. The study focused on identifying the conditions when visibly impact waves were formed by the like-on-like injector at elevated pressures. After identifying where the impact waves were easily identified, dynamic mode decomposition (DMD) was used to extract the natural frequency associated with the impact waves. The same condition was then subjected to high frequency acoustic forcing with incremental pressure amplitudes in both the PAN and PN configurations. High speed backlit imaging was used to capture the effect of acoustic forcing has on the impact waves. DMD analysis was performed to identify the dominate mode frequencies and structures.

## II. Experimental Set-up and Methods

The experiment was performed at Air Force Research Laboratory (AFRL), Edwards. A schematic of the experimental facility can be found in previous research conducted using shear coaxial injectors[12-13]. The same windowed pressure chamber from the previous shear coaxial injector studies was used for these studies. The impingement jet injector was manufacture as a cap disk that attaches to small reservoir. High machining tolerances

were kept on the cap to ensure proper jet impingement. A drawing of the cap and reservoir is shown in Figure 2. The natural acoustic frequencies of the reservoir are 16 kHz longitudinally and 35 kHz radially, both are higher than the forcing frequencies that were used for these studies. The impinging jet injector selected for this study has a jet diameter of 0.5 mm (0.02 in) with a half angle between exit holes of 30 degrees. Cryogenic nitrogen was used as the working fluid. The injector has a flow passage length of l/d of 8 within the injector. After exiting the injector, the fluid travels a pre-impingement length of 2.3 jet diameters. The jet velocity was controlled by varying the mass flow rate fed into the reservoir. A Porter mass flow meter (model 123-DKASVDAA) was used to measure the gaseous nitrogen flow. The gaseous nitrogen then traveled to a liquid nitrogen heat exchanger, where the gaseous nitrogen was converted to liquid nitrogen before entering the injector. An E type thermocouple on a piezo-electric translating stage (AttoCube ANS Scanners) was used to measure the temperature of the liquid impingement sheet prior to testing to ensure the temperature of the liquid nitrogen emerging from the injector was at steady state condition. A xenon arc lamp was used to provide the illumination for the back lit images. A high speed Phantom v710 CMOS camera, set at 25 kHz frame rate, was used to capture impact waves from the impingement sheet.

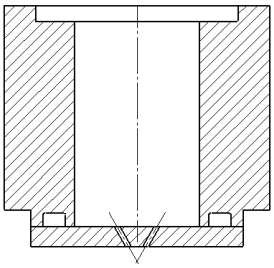

**Figure 2. Drawing of the injector cap attached to the liquid nitrogen feed reservoir.**

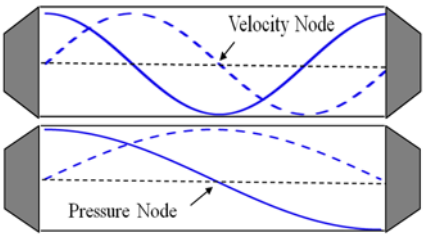


**Figure 3.** An instant in time of PAN and PN forcing. The solid line is the pressure fluctuations and the dash line is the velocity fluctuations. In PAN forcing, the injector experiences maximum and minimum pressure fluctuations. In PN forcing, the velocity fluctuations are maximum.

The acoustic waves used for the acoustic forcing portion of the study were generated by a Fluke 292 arbitrary waveform generator. The signal generator was then fed to two Trek PZD2000A high-voltage amplifiers that drove two piezo-sirens and generate a standing wave. The impingement sheet was then subjected to the acoustic forcing from the piezo-sirens tuned to the resonance chamber frequency for a PAN or PN configuration. Both the PAN and PN where centered at the middle of the impingement sheet. The shape of the PAN and PN forcing and be seen in Figure 3. For PAN forcing the pressure fluctuations are maximum and the velocity fluctuations are maximum for the PN forcing. Three differential pressure transducers (Kulite CCQ-093) were used to measure both the shape and amplitude of the acoustic forcing to ensure that a PAN and PN was achieved for each test condition. The chamber resonance for the PAN configuration was measured and driven at 2950 Hz and 3110 Hz for the PN. The impingement sheet was then subjected to incremental pressure amplitudes and the physical response was then visually recorded with the high speed camera. Dynamic mode decomposition (DMD), as outlined by Peter Schmid[14], was then used to extract the natural frequency of the impact waves in the unforced and forced conditions and their corresponding spatial response and structures.

## III. Results

### A. Velocity and Chamber Pressure Parametric Sweeps

For the first portion of the experiment, both jet velocity and chamber pressure were varied until visible impact waves became prominent on the impingement sheet. Impact waves appeared in a narrow range of conditions. Impact waves were observed at low jet velocities within the range of 2 to 5 m/s and at a chamber pressure of 1 to 1.37 MPa (150 to 200 PSIA) corresponding to jet Reynolds numbers of 7000 to 20000 and Weber numbers of 220 to 760, respectively. Figure 4 shows the spray formed by the impinging jets at several test conditions. Each column in Figure

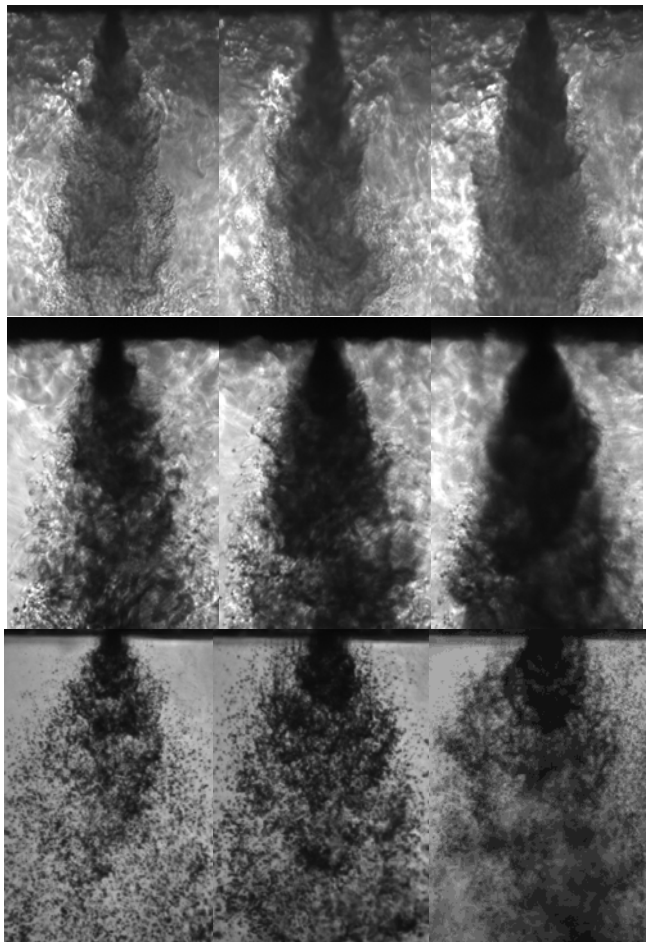

**Figure 4. The spray formed by the impinging jets. Each column the jet velocity if the same of 5, 7, and 10 m/s. The first row of images was taken at a supercritical chamber pressure of 4.8 MPa (700 Psia), the second and third row at subcritical pressures of 2.5 MPa (375 Psia) and 1.37 MPa (200 Psia).**

4 corresponds to the same jet velocity of 5, 7, and 10 m/s. The first row in Figure 4 is at a chamber pressure of 4.8 MPa (700Psia), above the supercritical pressure of nitrogen of 3.39 MPa (492 PSIA). The middle row and third row were taken at a subcritical chamber pressures of 2.5 MPa (375 PSIA) and 1.37 MPa (200 PSIA), respectively. At the supercritical chamber pressure a fine mist was formed regardless of the jet velocity and no evidence of impact waves was observed. As the chamber pressure is reduced to subcritical conditions, droplets and ligaments were observed to be shed off from the impingement sheet. No such identifiable droplets or ligaments were observed in the supercritical condition. As the jet velocity was increased for subcritical chamber pressure of 2.5 MPa, finer droplets were formed and eventually a dense mist was observed. A similar behavior was observed for the 1.37 MPa chamber pressure condition, but a dense mist similar to the 2.5 MPa and 10 m/s condition was never observed. It is apparent from these instantaneous images that there are different regimes of atomization for impinging jets which are dependent on several factors. At the supercritical condition it is possible that the aerodynamic forces on the cylindrical jets promptly atomize and form a fine mist or at these conditions the injection can no longer be regarded as an atomization or spray formation process. Further work will be require to understand how the interface between the low temperature jet and the supercritical nitrogen play a role, since the Weber number at these conditions approaches infinity and the mist formed is not as dense as the subcritical cases. At the subcritical conditions, chamber pressure or density ratio of the jet and the chamber gas plays a large role in promptly atomizing the impingement sheet, since it is evident that mist is formed at 10 m/s for the 2.5 MPa chamber pressure condition and not 1.37 MPa.

For the higher chamber pressure conditions above 1.4 MPa no discernible impact waves or frequencies were detected. It was only when the jet velocities were at 5 m/s and below and at 1.37MPa and below chamber pressures did impact waves became visually prominent. Figure 5 shows impact waves originating from the impingement point for the subcritical chamber pressures of 1 and 1.37 MPa at a constant jet velocity of 2 m/s. Similar to the higher jet

velocity conditions, as the chamber pressure is increased, evidence of impact wave structures on the impingement sheet breaks down and a dense mist is formed. It was also observed that there was lack of structure at the lower chamber pressures, evident in the lowest chamber pressure shown in Figure 5. From low jet velocity conditions, chamber pressures between 1 and 1.37 MPa produced the most prominent impact waves, particularly at 1 MPa shown in Figure 5. Although from Figure 5 the chamber pressure condition at 1 MPa shows evidence of impact wave atomization, the chamber pressure of 1.37 MPa was selected for further analysis with a constant jet velocity at 2 m/s. Based on the jet diameter the jet Reynolds number was 7800 and a jet Weber of 270, meeting the critical Weber number criteria calculated by Heidmann *et al*. The jet exit temperature was kept at a constant 95 K.

### B. Acoustic Forcing Results

Figure 6 is an instantaneous image of the impingement sheet without any acoustic forcing for a chamber pressure

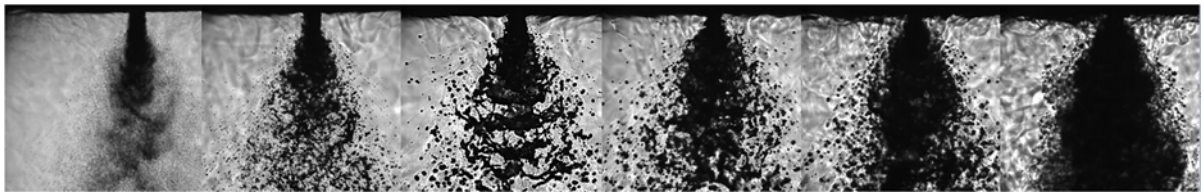

**Figure 5. Instantaneous images of the flow field of the impingement sheet at a constant jet velocity of 2 m/s and increasing chamber pressure. From left to right the chamber pressure if 0.34, 0.68, 1, 1.37, 2.06, 2.75 MPa. A density ratio of jet over chamber of 165, 78, 53, 38, 25, 19.**

of 1.37 MPa and a jet velocity of 2 m/s. The impact waves and subsequent ligaments formed are shown to be emanating from the impingement sheet. This condition, with no acoustic forcing, served as a reference to compare to the acoustic forcing conditions. Dynamic mode decomposition was used to extract the natural frequencies of the impact waves emanating from the impingement sheet. The DMD analysis was apply to red square section shown in Figure 6. The DMD amplitude spectrum is shown below in Figure 7. Although no dominant mode was detected by the DMD analysis, the natural frequency of the corresponding to impact waves was measured to 4822 Hz, based on visually inspecting the spatial DMD modes.

The DMD spatial mode corresponding to the impact waves for the base condition is shown in Figure 8. The alternating red and blue bands correspond to light intensity fluctuations due to dark liquid nitrogen impact waves passing on the exterior of the impingement sheet. It is currently suspected that variations in the impact wave's convective speeds or droplets shed along the exterior of the impingement sheet dampen the spectral content associated with impact waves and hence weak spectral frequency is picked up by the DMD analysis. The impact wave velocity is suspected because based on the high speed images, impact wave's velocity decelerates the further away they are from the impingement point. There is also a great degree of variation as to when the impact wave detach from the impingement sheet and is shed as ligaments. This variation of the breakup length of the impingement sheet seems to affect the impact wave velocity. A similar observation was made by Heidmann *et al* depending if the impingement sheet was closed or open rim. Heidmann *et al* also made an observation that the breakup length of the impingement

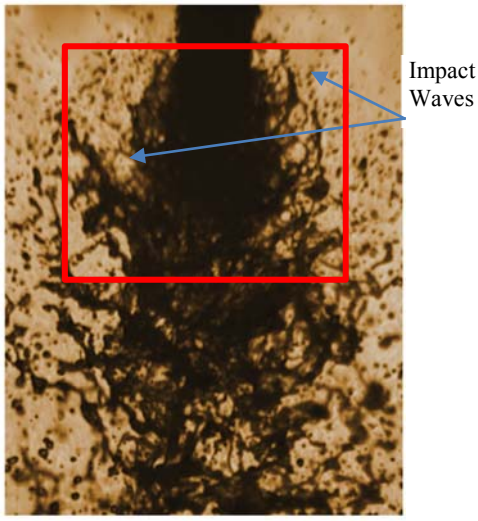


**Figure 6. Instantaneous image of the impingement with impact waves emanating from the impingement sheet.**

a) b)

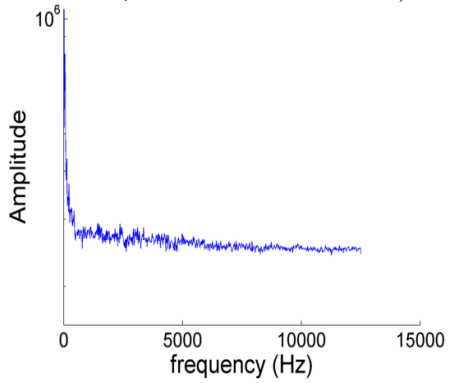


**Figure 7. DMD amplitude spectrum from the no forcing base condition.**

b)

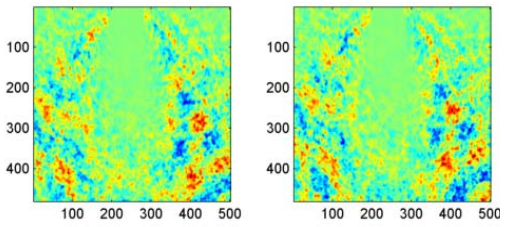


**Figure 8. DMD spatial for the base condition at 4822Hz. a) is the real portion and b) is the imaginary portion.**

sheet had a large variation in the fully develop mode and that the breakup length cannot be measured with any certainty. Similar mechanisms are likely responsible for the weak DMD amplitude of the impact waves since the impingement sheet in Figure 7 is in the fully developed regime, although further study will be needed to address the weak spectral strength.

Table 1 shows the acoustic test conditions with the pressure amplitude (P') the impingement sheet was subjected. Table 1 also has P' normalized to the dynamic pressure of the jets. For the PAN conditions, a total of 5 conditions were tested and a total of 4 conditions were tested for the PN configurations. For the PAN conditions, at the low P' (PAN 1 condition) acoustic forcing, the impingement sheet doesn't couple with the acoustic forcing. As P' is increased, the impingement sheet starts to couple with the acoustic forcing. This transition can be observed in the DMD amplitude spectrum shown in Figure 9. The corresponding DMD spatial mode is also shown. From Figure 9, PAN 1 condition is relatively unchanged when subjected to low P' PAN acoustic forcing. The DMD amplitude spectrum appears similar to the based unforced condition shown in Figure 7. The DMD spatial mode in Figure 9a also appears similar to the Figure 8 with the wave like pattern. Both PAN and the base condition have similar frequencies associated with the wave like pattern with frequencies of 4730 Hz and 4822 Hz, respectively, indicating this low level of acoustic forcing has little influence the dynamics of the impingement sheet and the frequency of the impact waves. The transition to where the impingement sheet couples with the acoustic forcing can be readily seen in the PAN 2 condition. Figure 9b shows the DMD amplitude spectrum with a peak centered at 2957 Hz, close to the acoustic forcing frequency of 2950 Hz. The DMD spatial mode, shown in Figure 9b, also demonstrates the transition with the impingement sheet. The alternating red and blue bands have grown larger and across the entire impingement sheet. This is different when from the base condition having the alternating bands only on exterior of the impingement sheet. What this transition seems to indicate that there is a coupling between the injector mass flow rate and the acoustic field. The impingement sheet under goes a surge of mass flow when the PAN forcing dips in the negative direction due to its sinusoid nature, it results in a temporally larger differential pressure This localized larger pressure differential drives a larger volume of mass flow through the injector. The impingement sheet also contracts in size when the PAN forcing is at its greatest and resulting in a small differential pressure between chamber and injector, thus restricting mass flow.

This coupling effect can be readily noticed for the PAN 5 condition, where the impingement sheet has fully coupled with the acoustic forcing. Both the DMD amplitude spectrum and spatial mode are shown in Figure 10. A strong peak centered at 2925 Hz, within less than 1% error of the acoustic forcing frequency of 2950Hz, is readily noticeable in Figure 10a, along with a higher harmonic. In Figure 10b demonstrates the large physical expansion and contraction of the impingement sheet, due to the surges of mass flow rates the injector is experiencing. It is at

**Table 1.** Acoustic Test conditions with relevant parameters.

| | **No Forcing** | **PAN 1** | **PAN 2** | **PAN 3** | **PAN 4** | **PAN 5** | **PN 1** | **PN 2** | **PN 3** | **PN 4** |
|---|---|---|---|---|---|---|---|---|---|---|
| P'(Psi) | 0 | 1.75 | 2.97 | 4.5 | 6.6 | 11 | 1.5 | 2.7 | 6.2 | 7.6 |
| $P'/\frac{1}{2}\rho u^2$ | 0 | 9.13 | 15.52 | 23.4 | 34.3 | 58.1 | 9.13 | 15.52 | 37.6 | 40 |

this condition that no traces of the impact waves were readily visible. Instead, what was observed was a large group of droplets shedding at the acoustic forcing frequency from the impingement sheet. This is indicative of a klystron effect, where faster moving fluid particles overtake slower liquid particles. This event is captured in the phase average images shown in Figure 11. The phased average images were false colored to best demonstrate both large group of droplets being shed and the klystron effect. As the pressure increases locally below the injector, there is a temporarily reduction in mass flow and jet velocity, afterwards the liquid jets

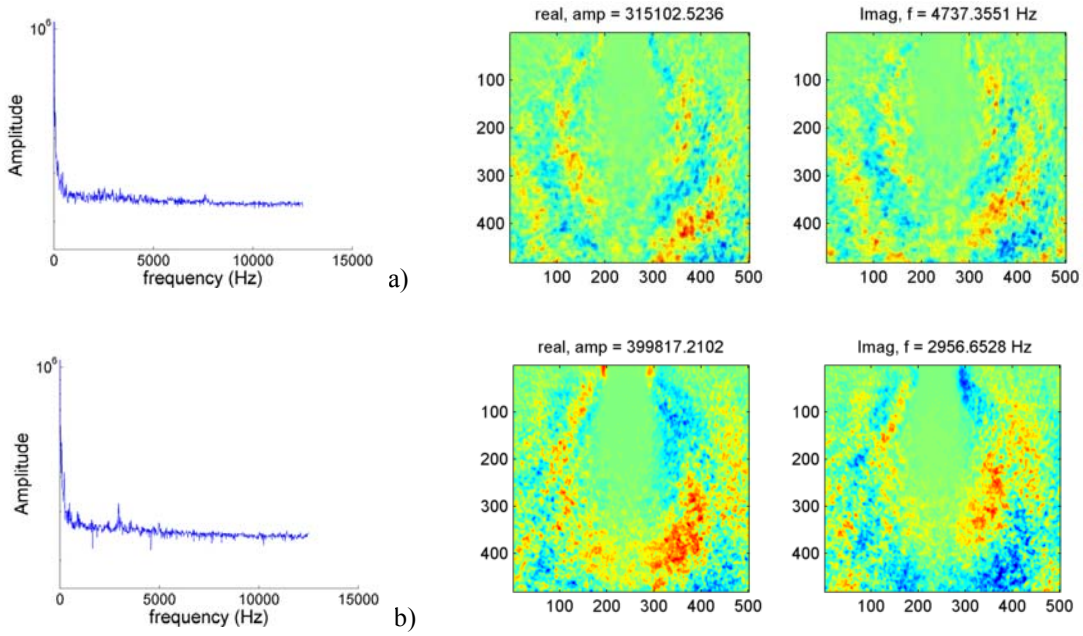


**Figure 9. The DMD amplitude spectrum with the corresponding spatial mode. A) is the DMD amplitude spectrum and spatial mode for PAN 1 condition. B) is the DMD amplitude spectrum and spatial mode for PAN 2 condition.**

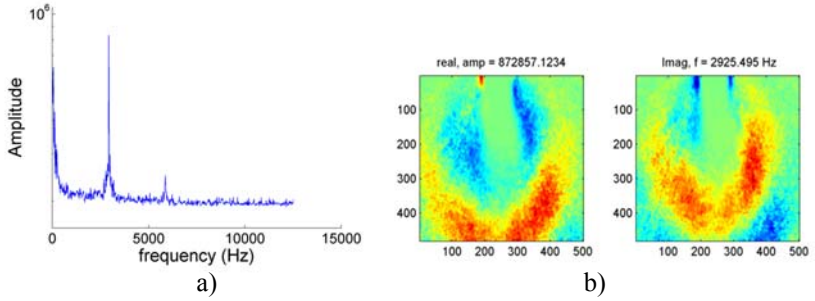


**Figure 10. DMD output for PAN 5. A) is the DMD amplitude spectrum and b) is the corresponding spatial mode of 2925 Hz.**

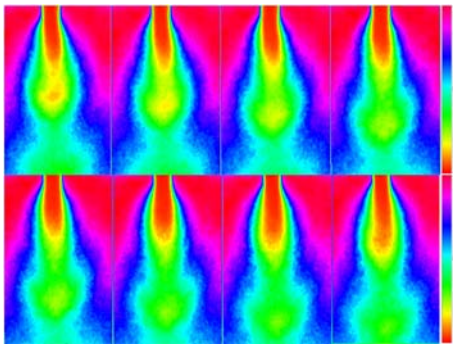

**Figure 11. False colored, phased average images of the PAN 5 condition. A large small of liquid nitrogen is shown being shed off.**

surge when the pressure amplitude dips. This dip in pressure temporally increases both the mass flow and jet velocity. This also gives the instantaneous images a "Christmas tree[15]" appearance (Appendix A). It is after when the pressure dips that the impingement sheet is observed to expand to its maximum width and shed large group of droplets. It is this condition where the atomization regime is dominant by the coupling of injector with the imposed acoustic field and not by impact waves. Based on observation of the high speed images no impact waves where formed when the injector fully coupled with the acoustic field. A similar coupling between the propellant feed system and the acoustic field has been identified since the Apollo era[8].

For the PN conditions, the velocity fluctuations are maximum, unlike the PAN conditions where the pressure fluctuations are maximum. For the PN conditions coupling between the acoustic perturbations and impingement sheet occurred at a lower pressure

amplitude. Figure 12 demonstrates this coupling at a lower pressure amplitude. Shown in Figure 12 is the DMD spectrum and spatial mode for the PN 1 and PN 4 conditions. Unlike the PAN conditions, the velocity perturbations produce an in plane flapping motion of the impingement sheet. Both PN conditions spatial modes share the same characteristic shape. As the pressure amplitude is increased the in plane flapping motion becomes more pronounce as shown from Figure 12b for PN 4 condition. Although the PN spatial modes appear similar to the base case condition, fundamentally they represent a different mode of operation. In the base condition the alternating red and blue pattern are symmetric along the impingement sheet. This is physically representative of impact waves travelling down along the impingement sheet. In the PN forcing, the spatial modes have an alternating patterns that are asymmetrical. Physically what is occurring is that in a PN acoustic field the two cylindrical jets swing in phase with the velocity perturbations. As they swing, the impingement point is physically displaced and hence the impingement sheet is also displaced resulting in the in plane flapping motion.

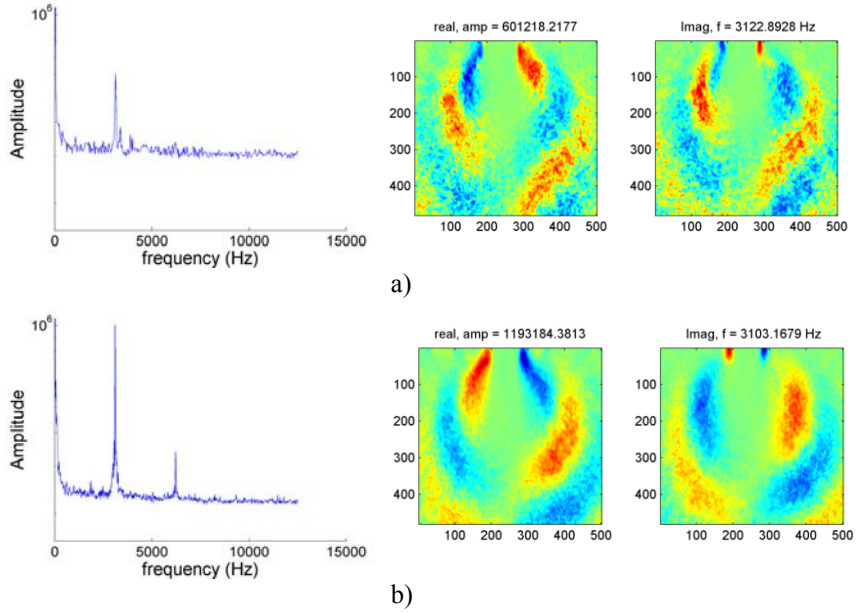


**Figure 12. The DMD spectrum and spatial mode for a) PN 1 and b) Pan 4.**

This in plane flapping motion is observed in the phased average images of PN 4 condition in Figure 13. Unlike the PAN forcing conditions where the cyclic mass flow variations produce a symmetric impingement sheet, PN forcing produces an S-shape curvature along the impingement sheet. S-shape curvature is indicative of the impingement point being periodically displaced. What was also observed was that ligaments would be shed in the direction of the incoming acoustic wave (Appendix A). This is a different mode of atomization when compared to the base condition. In the base condition the dynamic pressure of the liquid jets are used to overcome the surface tension force and atomize into droplets, but prior to becoming droplets, impact waves form on the impingement sheet and subsequently detach as ligaments and form droplets. Instead in a PN acoustic field, the edges of the impingement sheet are stripped off as ligaments and form a swig-swag pattern downstream. It is this mode of atomization that dominates the impingement sheet and not impact waves. Similar to PAN 5 condition, no impact waves were observed when the jets fully coupled with the acoustic field. It is believe that after a certain pressure amplitude associated with both PAN and PN acoustic forcing is reached, the impingement sheet is never fully developed, and hence limits any influence or traces of impact waves on the impingement sheet.

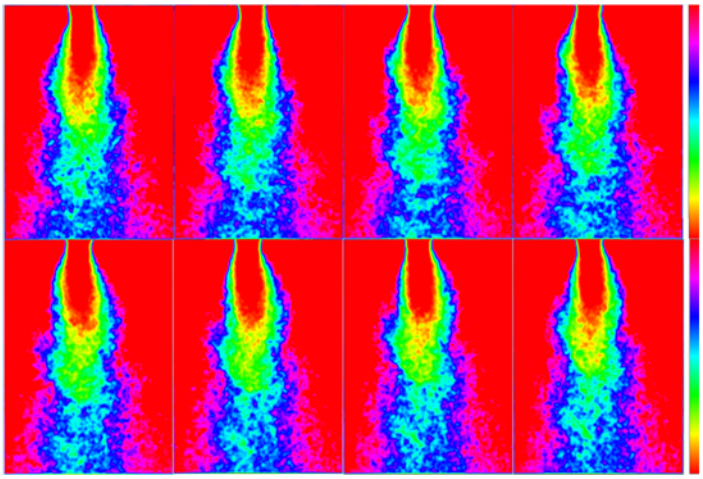

**Figure 13. False colored, phased average images of the PN 4 condition. An in plane flapping is generated with PN forcing.**

## IV. Conclusion

Cryogenic nitrogen impinging jets were studied under a high pressure environment and subjected to an acoustic perturbations. High speed, backlit imaging was used to capture the physical response of the impact waves to the acoustic forcing present on impingement sheet form. For the first phase of the study**,** jet velocity and chamber pressure were varied until impact waves were visually prominent on the impingement sheet. Chamber pressures, up to 4.8 MPa, and jet velocity, 2 to 10 m/s, were investigated. It was observed that impact waves became visually prominent in a narrow range of chamber pressures and jet velocities, particularly when both jet velocity and chamber pressure are low. At supercritical pressures, no droplets or ligaments were ever observed to form, instead the flow field resemble a fine mist. In subcritical pressure both ligaments and droplets were observed to be shed from the impingement sheet. In the subcritical pressures there appears to be an influence of jet to chamber gas density ratio. It was observed for the same jet velocity a transition to a fully atomize, when a dense mist is formed, occurs sooner at higher chamber pressures.

After the conditions that led to impact waves being visually prominent were identified, dynamic mode decomposition was used to extract the natural frequencies of impact waves and isolate the spatial structures, both the unforced and force conditions at a constant chamber pressure and jet velocity. For the forces conditions the pressure amplitude was incrementally increased until the injector and the acoustic field fully coupled. The results indicate that impact waves influence appear to vanish once a certain pressure amplitude is reached. When subjected to PAN forcing the impingement sheet size grows and decays and a large group of droplets are shed. For the PN forced conditions, in-plane flapping is generated and ligaments are stripped of the impingement sheet.

## References


[1]Anderson, W. E., Ryan, H. M., Pal, S., and Santoro, R. J., "Fundamental Studies of Impinging Liquid Jets," *30th Aerospace Sciences Meeting & Exhibit, AIAA Paper 92-0458, Reno, NV*.

[2]Anderson, W. E., Ryan, H. M., and Santoro, R. J., "Impinging Jet Injector Atomization," Liquid Rocket Combustion Instability, edited by V. Yang and W. E. Anderson, Progress in Astronautics and Aeronautics, vol. 169, AIAA, Washington D.C., 1995, pp. 215-246

[3]James, M. D., Kubal, T. D., Son, S. F., Anderson, W. E., and Poutpoint, T. L., " Calibration of an Impinging Jet Injector Suitbale for Liquid and Gelled Hypergolic Propellants," *45th AIAA/ASME/SAE/ASEE Joint Propulsion Conference & Exhibit*, Denver, Co, AIAA 2009-4882, 2009

[4]Fakhri, S., Lee, J. G., and Yetter, R. A., "Atomization and Spray Characteristics of Gelled-Propellant Simulants Formed by Two Impinging Jets," *45th AIAA/ASME/SAE/ASEE Joint Propulsion Conference & Exhibit*, Denver, Co, AIAA 2009-5241, 2009

[4] Heidmann, M. F., Priem, R. J., and Humphrey, J. C., "A Study of Sprays Formed by Two Impinging Jets," NACA TN-3835, 1957.

[5] Dombrowski, N., and Hooper, P. C., " A Study of the Sprays Formed Imping Jets in Laminar and Turbulent Flow," *Journal of Fluid Mechanics,* vol. 18, no. 3, 1964, pp. 392-400.

[6] Anderson, W. E., Ryan, H. M., and Santoro, R. J., "Impinging Jet Injector Atomization," Liquid Rocket Combustion Instability, edited by V. Yang and W. E. Anderson, Progress in Astronautics and Aeronautics, vol. 169, AIAA, Washington D.C., 1995, pp. 215-246

[7] Anderson, W. E., Ryan, H. M., Pal, S., and Santoro, R. J., "Spray Formation Processes of Impinging Jet Injectors," NASA Propulsion Engineering Research Center, vol. 2, N94-23042, 1993, pp.69-74.

[8] Li, R., and Ashgriz., "Characteristics of liquid sheets formed by two impinging jet," *Physics of Fluids*, Vol. 18, No. 8, 2006, pp. 087104-1, 087104-13

[9] Ciezki, H. K., Tiedt, T., Von Kampen, J., and Bartels, Nora., "Atomization Behavior of Newtonian Fluids with an Impinging Jet Injector in Dependence upon Reynolds and Weber Numbers" *41th AIAA/ASME/SAE/ASEE Joint Propulsion Conference and Exhibit*, Tucson, AZ, AIAA 2005-4477, 2005.

[10] Anderson, W. E., Ryan, H. M., and Santoro, R. J., "Impact Wave-Based Model of Impinging Jet Atomization," *Atomization and Sprays*, Vol. 16, No. 7, 2006, pp. 791-806

[11] Chen, X., Ma, D., and Yang, V., "Mechanism Study of Impact Wave in Impinging Jets Atomization," *50th AIAA Aerospace Sciences Meeting*, Nashville, TN, AIAA 2012-1089, 2012

[12] Teshome, S., Leyva, I. A., Talley, D, G., and Karagozian, A. R., "Cryogenic High-Pressure Shear-Coaxial Jets Exposed to Transverse Acoustic Forcing," *50th Aerospace Sciences Meeting*, Nashville, TN, AIAA2012-12665, 2012

[13] Graham, J. J., Leyva, I. A., Rodriguez, J. I., and Talley, D. G., "On the Effect of a Transverse Acoustic Field on a Flush Shear Coaxial Injector," *45th AIAA/ASME/SAE/ASEE Joint Propulsion Conference and Exhibit*, Denver, CO, AIAA 2009-5142, 2009

[14] Schmid, P. J., "Dynamic mode decomposition of numerical and experimental data," *Journal of Fluid Mechanics*, Vol. 656, 2010, pp. 5-28

[15]Harrje D. T., and Reardon, F. H., "Liquid Propellant Rocket Combustion Instability," NASA SP-194, 1972

## V. Appendix A

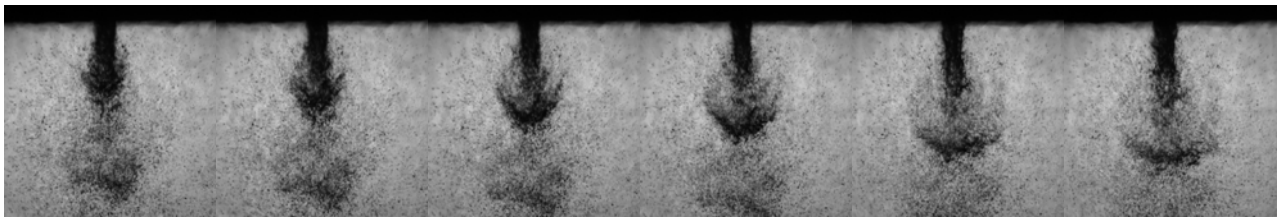

**Figure A1. Instantaneous images of an acoustic cycle for the PAN 5 condition. A large group of are shed and no impact waves were ever observed. The klystron effect produces the Christmas tree shape in the far left image.**

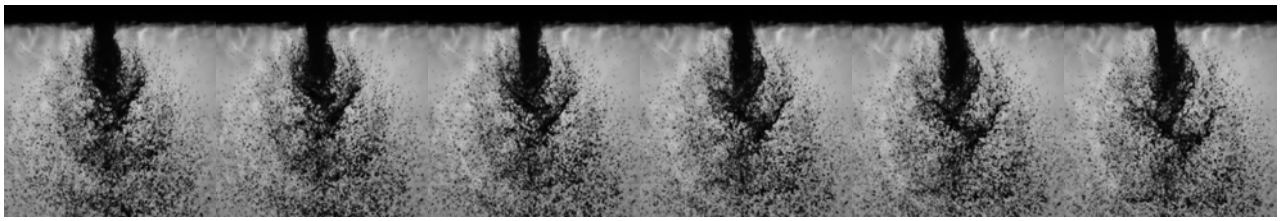

**Figure A2. Instantaneous image of an acoustic cycle for the PN 4 condition. A swig-swag pattern of ligaments being shed off the impingement sheet can be observed in the downstream flow. No impact waves were ever observed in this condition.**